Atmos. Meas. Tech. Discuss., 7, 8777–8816, 2014
www.atmos-meas-tech-discuss.net/7/8777/2014/
doi:10.5194/amtd-7-8777-2014


Atmospheric Measurement Techniques Discussions
Open Access



# Impacts of cloud heterogeneities on cirrus optical properties retrieved from spatial thermal infrared radiometry

**T. Fauchez[1], P. Dubuisson[1], C. Cornet[1], F. Szczap[2], A. Garnier[3,4], and J. Pelon[5]**

[1]Laboratoire d'Optique Atmosphérique, Université Lille 1, Villeneuve d'Ascq, France
[2]Laboratoire de Météorologie Physique, Université Blaise Pascal, Clermont Ferrand, France
[3]Science Systems and Applications, Inc., Hampton, Virginia, USA
[4]NASA Langley Research Center, Hampton, Virginia, USA
[5]Laboratoire Atmosphères, Milieux, Observations Spatiales, UPMC-UVSQ-CNRS, Paris, France

Received: 20 May 2014 – Accepted: 18 July 2014 – Published: 27 August 2014

Correspondence to: C. Cornet (celine.cornet@univ-lille1.fr)

Published by Copernicus Publications on behalf of the European Geosciences Union.

## Abstract

This paper presents a study, based on simulations, of the impact of cirrus cloud heterogeneities on the retrieval of cloud parameters (optical thickness and effective diameter) for the Imaging Infrared Radiometer (IIR) on board CALIPSO. Cirrus clouds are generated by the stochastic model 3DCLOUD for two different cloud fields and for several averaged cloud parameters. One is obtained from a cirrus observed on the 25 May 2007 during the airborne campaign CIRCLE-2 and the other is a cirrus uncinus. The radiative transfer is simulated with the code 3DMCPOL. To assess the errors due to cloud heterogeneities, two related retrieval algorithms are used: (i) The split window technique to retrieve the ice crystal effective diameter and (ii) an algorithm similar to the IIR operational algorithm to retrieve the effective emissivity and the effective optical thickness. Differences between input parameters and retrieved parameters are compared as a function of different cloud properties such as the mean optical thickness, the heterogeneity parameter and the effective diameter. The optical thickness heterogeneity for each 1 km × 1 km observation pixel is represented by the optical thickness standard deviation computed using 100 m × 100 m subpixels. We show that optical thickness heterogeneity may have a strong impact on the retrieved parameters, mainly due to the Plane Parallel Approximation (PPA). In particular, for cirrus cloud with ice crystal size of approximately 10 µm, the averaged error on the retrieved effective diameter is about 2.5 µm (∼ 25 %) and on the effective optical thickness of about −0.20 (∼ 12 %). Then, these biases decrease with the increase of the ice effective size due to a decrease of the cloud absorption and thus of the PPA bias. Cloud heterogeneity effects are much more higher than other possible sources of error. They become larger than the retrieval incertitude of the IIR algorithm from a standard deviation of the optical thickness, inside the observation pixel, superior to 1.





AMTD

7, 8777–8816, 2014

## 1 Introduction

In the context of global climate change, the representation and role of clouds are still uncertain. For example, ice clouds play an important role in the climate and on the Earth's radiation budget (Liou, 1986). Cirrus clouds lead mainly to a positive radiative forcing due to their high temperature contrast with regard to the surface. However, the cirrus radiative forcing could depend on the cirrus optical thickness, altitude and ice crystal effective size (Katagiri et al., 2013). Consequently, to improve our knowledge, it is essential to assess the feedback and climate effects of these clouds (Stephens, 1980). Global observations are well adapted to follow and better understand cloud evolution and characteristics. In this context, several spatial missions have been initiated. One of the most important is the A-train spatial mission composed of several complementary instruments being able to observe clouds quasi-simultaneously. In this work, we focus on the infrared radiometry such as measurements obtained by the passive instruments IIR (Infrared Imaging Radiometer, Garnier et al., 2012, 2013) on board the satellite CALIPSO or MODIS (Moderate Resolution Imaging Spectrometer, Platnick et al., 2003) on board the platform AQUA.

From radiometric measurements, dedicated operational algorithms allow retrieving cloud properties such as optical thickness and ice crystal effective diameter for each pixel of the cloudy scene. Because of operational constraints (lack of information regarding the three dimensional (3-D) structure of the atmosphere, time constraints, etc.), retrieval algorithms assume that clouds are homogeneous and infinite between two planes. This assumption of a one dimensional (1-D) radiative transfer is called the homogeneous *Independent Pixel Approximation* (IPA, Cahalan et al., 1994) or *Independent Column Approximation* (ICA, Stephens et al., 1991). However, real clouds can be far from this simplified model and this assumption may lead to biases on the retrieval of clouds properties (Fauchez et al., 2014).

In a real atmosphere, clouds show, indeed, 3-D structures with heterogeneities and the radiative transfer occurs in the three dimensions. In the solar spectral range, many





AMTD
7, 8777–8816, 2014

studies have been conducted concerning the impact of cloud heterogeneities on the cloud products. These studies primarily concern warm clouds such as strato-cumulus (Varnai and Marshak, 2001; Zinner and Mayer, 2006; Kato and Marshak, 2009, etc.). The authors showed that the sign and the amplitude of the errors depend on numerous factors, such as the spatial resolution, the wavelength, the geometry of observation and the cloud type (cloud dimensions, microphysical and macrophysical variabilities). Concerning cirrus clouds, Fauchez et al. (2014) shows that cirrus cloud heterogeneities lead to non-negligible effects on Brightness Temperatures (BT) and that these effects mainly depend on the standard deviation of the optical thickness inside the observation pixel. The retrieval of cloud properties using radiances or BT may thus be impacted by the heterogeneity effects. Therefore, in this work, we go further and investigate the impact of cirrus heterogeneities on the retrieved cloud products. This study is conducted from simulations of radiometric measurements of IIR in three typical spectral bands, 8.65, 10.60 and 12.05 µm.

The method used to retrieve cloud products depends on the spectral domain. Indeed, in the thermal infrared atmospheric window (8–13 µm), cloud optical properties (optical thickness and ice crystal effective size) are retrieved using the SWT Split Window Technique (Inoue, 1985; Parol et al., 1991; Dubuisson et al., 2008). This method is generally limited to thin cirrus clouds (optical thickness below approximately 3 at 532 nm) and small crystals (effective diameters below approximately 40 µm). In the visible and near-infrared ranges, cloud optical properties are commonly retrieved using the Nakajima and King method (NK, Nakajima and King, 1990). This method combines measurements in visible and near-infrared channels for thicker cirrus clouds and larger ice crystals. Cooper et al. (2007) combined these two methods for MODIS measurements to treat thin and thick cirrus in the same time.

The paper is organized as follows. In Sect. 2, we present a short description of the modelling tools used in this study: (i) the cloud generator 3DCLOUD (Szczap et al., 2014), (ii) the radiative transfer code 3DMCPOL (Cornet et al., 2010; Fauchez et al., 2014) and (iii) two related retrieval algorithms. The Sect. 3 presents, from simulations, the possible errors due to the 1-D approximation on the retrieved optical properties. The Sect. 4 compares heterogeneity effects with other possible sources of errors on the retrieved products. Conclusions and perspectives are given in Sect. 5.

## 2 Numerical models

### 2.1 3-D Ice Water Content generation

The stochastic model 3DCLOUD (Cornet et al., 2010; Szczap et al., 2014) is employed to generate realistic 3-D cirrus clouds. This model uses a simplified dynamical and thermodynamical approach to generated heterogeneous 3-D clouds as well as a Fourier transform framework to constrain scale invariant properties (Hogan and Kew, 2005; Szczap et al., 2014). Two different cirrus fields were simulated (Fig. 1) in a Mid-latitude Summer (MLS) atmosphere.

The first cirrus field has been modeled from meteorological profiles presented by Starr and Cox (1985) with the addition of a wind profile to form virgas. Different values of mean cloud parameters are used: the cirrus mean optical thickness $\tau_\mathrm{c}$, $\sigma_{\tau_\mathrm{c}}$ the standard deviation of the optical thickness on the entire field, the cirrus heterogeneity parameter $\rho_\tau = \sigma_{\tau_\mathrm{c}}/\tau_\mathrm{c}$ (Szczap et al., 2000) and the ice crystal effective diameter $D_\mathrm{eff}$. Eight cirrus with different mean cloud parameters are generated (Table 1) with parameters covering the characteristics of usual cirrus clouds (Sassen and Cho, 1992; Szczap et al., 2000; Carlin et al., 2002; Lynch et al., 2002). Note that the effective diameter of cirrus 3 to 5 ($D_\mathrm{eff}$ = 9.95 µm) is probably too small for cirrus with a mean optical thickness of 1.80 as, aggregations processes tend to increase the effective size (Fig. 12 of Garnier et al., 2013). However, cirrus 3 to 5 are useful to understand how heterogeneity effects increase with the mean optical thickness. The first cloud structure is presented in Fig. 1a and b. Figure 1a presents the 10 km × 10 km optical thickness field at 12.05 µm with a spatial resolution of 100 m and Fig. 1b the $x$–$z$ view of the Ice Water Content (IWC) of cirrus 3.





AMTD
7, 8777–8816, 2014

The second cirrus structure (Fig. 1c and d) is generated from measurements of the cirrus observed on the 25 May 2007 during the CIRCLE-2 airborne campaign (Mioche et al., 2010). In situ measurements provided by the aircraft as well as IIR radiometric measurements (mean optical thickness and mean heterogeneity parameter) are used as input of 3DCLOUD. In addition, we used meteorological data provided by the European Center for Medium-Range Weather Forecasts (ECMWF) to constrain the meteorological profiles (wind speed and orientation, temperature, humidity etc.). The scale invariant properties of every cirrus presented in Table 1 are controlled by a $-5/3$ constant spectral slope for all scales and altitude levels. This agree with the spectral slope of the backscattering coefficient measured at 532 nm at different altitudes by the LIDAR CALIOP/CALIPSO and the extinction coefficient measured by the Polar Nephelometer at the aircraft altitude (Fauchez et al., 2014).

## 2.2 Optical property parametrization

Cirrus optical properties are difficult to handle because of the diversity of crystal sizes, shapes and orientations in a cirrus cloud. Several parametrization were elaborated for visible and infrared wavelengths (Magono, 1966; C.-Labonnote et al., 2000; Yang et al., 2001, 2005; Baum et al., 2005, 2011; Baran and Labonnote, 2007; Baran et al., 2009, 2013; Baran, 2012). For cirrus 1 to 8, we employ the ice crystal model with aggregate crystal shape and a mono-disperse distribution used in the IIR retrieval algorithm (Garnier et al., 2013) and developed by Yang et al. (2001, 2005). This model gives an extinction coefficient, a single scattering albedo and an asymmetry factor (Yang et al., 2001, 2005). We use the phase function of Henyey and Greenstein (1940) which is sufficient, in the thermal infrared, to approximate the scattering (Yang et al., 2001). For these cirrus, the optical properties are constant over the entire cloud.

In order to generate 3-D-Dimensional and heterogeneous optical properties field, we use for the CII-1 and CII-2 cirrus, the parametrization of Baran et al. (2009, 2013) and Baran (2012). This parametrization gives, for each cloudy cell, the optical coefficients from the (IWC, Temperature) couple. These relations have been obtained from in situ





AMTD
7, 8777–8816, 2014

measurements of more than 20 000 Particle Size Distributions (PSD) (Field et al., 2005, 2007).

### 2.3 TOA brightness temperatures simulations.

TOA brightness temperatures in the three IIR thermal infrared channels (8.65 µm, 10.60 µm and 12.05 µm) are simulated with the 3DMCPOL code developed in the visible range by Cornet et al. (2010) and extended to the infrared range by Fauchez et al. (2014). 3DMCPOL is a forward Monte-Carlo algorithm using the Local Estimate Method (LEM, Marshak and Davis, 2005; Mayer, 2009) and being able to simulate radiances and brightness temperatures from the visible to the infrared range, including the polarization. The atmosphere is subdivided in voxels (3-D pixels), with a constant horizontal size ($\mathrm{d}x$, $\mathrm{d}y$) and a variable vertical size $\mathrm{d}z$. Each of them is described by the extinction coefficient $\sigma_\mathrm{e}$, the single scattering albedo $\varpi_0$, the phase function and the cloud temperature $T_\mathrm{c}$.

3-D BT are first simulated at the spatial resolution of 100 m × 100 m and then averaged to the IIR spatial resolution of 1 km × 1 km ($\mathrm{BT3D}_{1\,\mathrm{km}}$). 1-D BT are obtained by averaging cloud properties at 1 km × 1 km before simulating BT ($\mathrm{BT1D}_{1\,\mathrm{km}}$).

### 2.4 Retrieval algorithms of cloud parameters

Two related algorithms are used to retrieve cloud products: the Split-Window Technique (SWT, Inoue, 1985; Parol et al., 1991; Dubuisson et al., 2008) to retrieve the effective diameter and an algorithm similar to the IIR operational algorithm to retrieve the effective emissivity and the effective optical thickness.

In the thermal infrared atmospheric window, the SWT is one the most used method to retrieve the effective diameter and the cloud optical thickness using the difference of brightness temperatures between two thermal infrared channels (Parol et al., 1991; Radel et al., 2003; Dubuisson et al., 2008; Garnier et al., 2012, 2013). Figure 2 presents examples of arches for three Brightness Temperature Difference (BTD) as a function





AMTD
7, 8777–8816, 2014

of the BT of the channel 12.05 µm ($BT_{12}$) and for several effective diameters ($D_{\mathrm{eff}}$). The optical thickness decreases along each arches from the opaque cloud BT to the clear sky BT. Each arch corresponds to an effective size and the BTD decreases with the increase of the particle size. The sensitivity of the SWT to large particles ($D_{\mathrm{eff}} > 40$ µm) is weak. This is one of the main disadvantages of this method which can only accurately determines the effective size of particles under approximately 40 µm for cirrus clouds with an optical thickness approximately between 0.5 and 3 (Dubuisson et al., 2008; Sourdeval et al., 2012). Dubuisson et al. (2008) also show that the retrieval accuracy of the ice crystal effective diameter is included between 10–25 % and it is about 10 % for the optical thickness. We note that, the amplitude of $BTD_{8-10}$ arches is significantly smaller than the two others because its sensitivity on $D_{\mathrm{eff}}$ is weaker. Consequently, this channel pair will not be used in this study.

The IIR operational algorithm (Garnier et al., 2012) uses, as the SWT, radiance differences between channels but in a different way. Intermediate products (effective emissivity, effective optical thickness and microphysical indices) are computed to retrieve the ice crystal effective diameter and shape. The effective emissivity refers to the contribution of scattering in the retrieved emissivity, especially for small ice crystals in the band at 8.65 µm. One of the major interest of using the effective emissivity is its independence to cloud top altitude or geometrical thickness, contrary to brightness temperature differences used in the SWT. The effective emissivity $\varepsilon_{\mathrm{eff},k}$, for the channels $k$, is defined as:

$$\varepsilon_{\mathrm{eff},k} = [R_k - R_{k,\mathrm{BG}}]/[B_k(T_\mathrm{c}, Z_\mathrm{c}) - R_{k,\mathrm{BG}}], \tag{1}$$

with $R_k$, the measured (or simulated) radiance in the channel $k$; $R_{k,\mathrm{BG}}$, the measured (or simulated) radiance at TOA for clear sky; $B_k(T_\mathrm{c}, Z_\mathrm{c})$ the radiance of an opaque cloud (black body) localized at the centroid altitude of reference $Z_\mathrm{c}$ and at the centroid temperature $T_\mathrm{c}$ provided from the GEOS-5 model (Rienecker et al., 2008). The layer centroid altitude is a weighted average altitude based on the attenuated backscattered intensity of the LIDAR signal at 532 nm (Vaughan et al., 2009). Note that, in this study, we set the centroid altitude to the geometrical middle of the cloud.

The effective optical thickness $\tau_{\mathrm{eff},k}$ is then calculated as:

$$\tau_{\mathrm{eff},k} = -\ln(1 - \varepsilon_{\mathrm{eff},k}). \tag{2}$$

From $\tau_{\mathrm{eff},k}$, the microphysical indices $\mathrm{MI}^{12/8}$ and $\mathrm{MI}^{12/10}$, are defined as the ratio of $\tau_{\mathrm{eff},k}$ between the two channels (12.05 µm and 8.65 µm) and (12.05 µm and 10.60 µm) respectively:

$$\mathrm{MI}_{12/8} = \tau_{\mathrm{eff},12}/\tau_{\mathrm{eff},8}; \quad \mathrm{MI}_{12/10} = \tau_{\mathrm{eff},12}/\tau_{\mathrm{eff},10} \tag{3}$$

These microphysical indices strongly depend on microphysical and optical properties of the cloud layer. They depend, thus, mainly on the effective diameter and shape of ice crystals. From a Look Up Table pre-calculated by the FASDOM code (Dubuisson et al., 2005), two values of effective diameters $D_{\mathrm{eff}\,1\,\mathrm{km}}(10,8)$ and $D_{\mathrm{eff}\,1\,\mathrm{km}}(12,8)$ are obtained for each shape of particles (aggregates, plates, solid columns) considered in the IIR retrieval algorithm. The shape corresponding to the lowest difference between the two $D_{\mathrm{eff}\,1\,\mathrm{km}}$ is selected. The IIR operational algorithm uses, for the computation of optical properties, the Yang et al. (2001, 2005) model with a mono-modal effective diameter distribution.

We checked that errors due to the retrieval methods, estimated by comparing retrieved optical properties with optical properties used in the radiative transfer (not presented here), are less than 2 % on the effective diameter retrieved with the SWT and 4 % on the effective optical thickness retrieved with the algorithm similar to the IIR operational algorithm.

## 3 Impact of cirrus heterogeneities on the retrieved parameters

In this section, we present the heterogeneity effects on the retrieved products at the IIR spatial resolution of 1 km × 1 km according to different cloud properties (optical thickness, optical and microphysical properties, cirrus top altitude and geometrical thickness). The heterogeneity effects on retrieved parameters are assessed by using the difference between products retrieved from Brightness Temperatures computes at 1 km × 1 km in 3-D ($BT3D_{1\,km}$) and in 1-D ($BT1D_{1\,km}$).

In order to estimate the heterogeneity effects on the retrieved cloud products, we define the following errors due to cloud heterogeneities:

- $\Delta\varepsilon_{eff} = \varepsilon 3\text{-}D_{eff} - \varepsilon 1\text{-}D_{eff}$: on the effective emissivities calculated by the Eq. (1).
- $\Delta\tau_{eff} = \tau 3\text{-}D_{eff} - \tau 1\text{-}D_{eff}$: on the effective optical thicknesses calculated by the Eq. (2).
- $\Delta MI^{12/8} = MI3D^{12/8} - MI1D^{12/8}$ and $\Delta MI^{12/10} = MI3D^{12/10} - MI1D^{12/10}$: on the microphysical indices calculated from the Eq. (3).
- $\Delta D_{eff\,1\,km} = D_{eff}3D_{1\,km} - D_{eff}1D_{1\,km}$: on the ice crystal effective diameter retrieved with the SWT.

The index "3-D" corresponds to optical properties retrieved from $BT3D_{1\,km}$ and the index "1-D", to those retrieved from $BT1D_{1\,km}$. $\tau_{1\,km}$ is the optical thickness used in the radiative transfer simulation. $Deff1D_{1\,km}$ corresponds either to the effective diameter used in the radiative transfer simulation, when is known (cirrus 1 to 8 and CII-3), or to the effective diameter retrieved from $BT1D_{1\,km}$ when ice crystal effective diameters used in the radiative transfer simulation are unknown as for cirrus CII-1 and CII-2.

Heterogeneity impacts due to the optical thickness variability are discussed Sect. 3.1 and those due to optical and microphysical property variabilities in Sect. 3.2.

### 3.1 Heterogeneity impacts due to the optical thickness variability

Fauchez et al. (2014) show that $BT3D_{1\,km}$ are larger than $BT1D_{1\,km}$ and that their difference is well correlated with the standard deviation of the optical thickness inside the 1 km × 1 km observation pixel $\sigma_{\tau_{1\,km}}$. This brightness temperature difference is due to the Plane Parallel Approximation (PPA) caused by the non linearity of the relation between brightness temperature and optical thickness. The PPA is greater for highly absorbing bands because the increase of cloud absorption leads to a larger brightness temperature contrast between the cirrus top and the clear sky atmosphere and, thus, to a stronger averaging effect.

The Fig. 3 illustrates how cirrus heterogeneities affect the retrieval of the effective diameter and the optical thickness. The red arrow represents the BTD and BT values obtained with an homogeneous cloud with $D_{\mathrm{eff}}1\mathrm{D}_{1\,\mathrm{km}}$ and $\tau 1\mathrm{D}_{1\,\mathrm{km}}$. Using 3-D radiative transfer inside a heterogeneous cloud with the same mean properties, we obtained the BTD and BT values represented by the blue arrow in the Fig. 3. As heterogeneity effects are larger for the band at 12.05 µm than at 8.65 µm, Brightness Temperature Differences $\mathrm{BTD}_{8-12}$, first simulated at the spatial resolution of 100 m and then averaged to the IIR spatial resolution of 1 km, are smaller than those retrieved from radiances directly simulated at the spatial resolution of 1 km. Consequently, as effective diameters increase with the decrease of BTD, the retrieved $D_{\mathrm{eff}}3\mathrm{D}_{1\,\mathrm{km}}$ are larger than the mean value $D_{\mathrm{eff}}1\mathrm{D}_{1\,\mathrm{km}}$. In addition, the retrieved optical thicknesses $\tau 3\mathrm{D}_{1\,\mathrm{km}}$ are smaller than the mean optical thickness $\tau 1\mathrm{D}_{1\,\mathrm{km}}$.

In addition, Fig. 4 shows the effective emissivity as a function of the effective optical thickness estimated at the spatial resolution of 100 m. The relation between effective emissivities and effective optical thicknesses is no linear, as between brightness temperatures and optical thicknesses. Because of the PPA, the average of effective emissivities ($\overline{\varepsilon_{\mathrm{eff}}}$) is smaller than the effective emissivity of the average of effective optical thicknesses $\overline{\tau_{\mathrm{eff}}}$. Similarly to brightness temperatures, effective emissivities and effective optical thicknesses retrieved from radiances, first simulated at the spatial resolution of 100 m and then averaged to the IIR spatial resolution of 1 km, are smaller than those retrieved from radiances directly simulated at the spatial resolution of 1 km.

Figure 5 presents $\Delta\varepsilon_{\mathrm{eff}}$ (a, b and c) and $\Delta\tau_{\mathrm{eff}}$ (d, e and f) as a function of the standard deviation of the optical thickness inside the 1 km × 1 km observation pixel ($\sigma_{\tau_{1\,\mathrm{km}}}$) for cirrus 1 to 5 and for the bands at 8.65 µm, 10.60 µm and 12.05 µm respectively.





AMTD
7, 8777–8816, 2014

We notice, first of all, that $\Delta\varepsilon_{\text{eff}}$ and $\Delta\tau_{\text{eff}}$ are correlated with $\sigma_{\tau_{1\,\text{km}}}$ at more than 94 %, except for cirrus 1 at 8.65 µm where the horizontal transport smooths the slight heterogeneity of the radiative field. $\Delta\varepsilon_{\text{eff}}$ and $\Delta\tau_{\text{eff}}$ are negatives meaning that the 3-D effective emissivities and effective optical thicknesses are weaker than those in 1-D. Indeed, as explained by Fauchez et al. (2014), heterogeneity effects lead to an increase of radiances or brightness temperatures. As radiances decrease with the cloud extinction, larger radiances lead then to smaller cloud effective emissivity and effective optical thickness. In addition, we can see that $\Delta\varepsilon_{\text{eff}}$ and $\Delta\tau_{\text{eff}}$ depend on the wavelength. For example, at $\sigma_{\tau_{1\,\text{km}}} = 1$, $\Delta\varepsilon_{\text{eff}}$ is equal to −0.01 at 8.65 µm, −0.03 at 10.60 µm and −0.05 at 12.05 µm. This is due to the increase of absorption from 8.65 µm to 12.05 µm which leads to an increase of the contrast between cloud and clear sky pixels and thus to an increase of the PPA bias. For comparison, Garnier et al. (2012) shown that the error on the effective emissivity due to the retrieval method is of about 0.03 for the band at 12.05 µm (black lines of the Fig. 5) for an uncertainty of 1 K on the temperature of the clear sky atmosphere (case above an ocean). This incertitude is smaller than the average error due to cloud heterogeneity $\overline{\Delta\varepsilon_{\text{eff}}}$. We can note that, at $\sigma_{\tau_{1\,\text{km}}} \sim 1$, $\Delta\varepsilon_{\text{eff}}$ is equal or superior to 0.03 for bands at 10.60 µm and 12.05 µm. $\sigma_{\tau_{1\,\text{km}}} \sim 1$ corresponds also to the limit where the heterogeneity effects on brightness temperatures becomes superior to the IIR instrumental accuracy of 1 K (Fauchez et al., 2014).

Figure 6a and b represent respectively the error on the microphysical indices $\Delta\text{MI}^{12/8}$ and $\Delta\text{MI}^{12/10}$ as a function of $\sigma_{\tau_{1\,\text{km}}}$ for cirrus 1 to 5. We first notice, that the errors on the two microphysical indices are, on average, negatives, except again for cirrus 1 for $\Delta\text{MI}^{12/8}$. They increase with the cirrus mean optical thickness (from cirrus 1 to 3) and heterogeneity parameter (from cirrus 3 to 5). The correlation with $\sigma_{\tau_{1\,\text{km}}}$ is better for $\Delta\text{MI}^{12/10}$ than for $\Delta\text{MI}^{12/8}$. Again, the strongest scattering in the band at 8.65 µm tends to smooth the radiative field heterogeneities and, therefore, to degrade the correlation between $\Delta\text{MI}^{12/8}$ and $\sigma_{\tau_{1\,\text{km}}}$. $\Delta\text{MI}^{12/8}$ is, on average, larger than $\Delta\text{MI}^{12/10}$ because the difference of absorption and effective emissivity is significantly greater for the couple

12.05 µm/8.65 µm than for 12.05 µm/10.60 µm. As the effective diameters of ice crystals are estimated from the microphysical indices using a LUT, they are, thus, also impacted by heterogeneity effects. Retrieved effective diameters are expected to be too large, as microphysical indices are smaller in 3-D than in 1-D.

Using the SWT, we are also able to simulate the impact of cirrus heterogeneities on the retrieved effective diameters of ice crystals. In Fig. 7, we plot the error on the effective diameter $\Delta D_{\mathrm{eff\,1\,km}}$, due to heterogeneities, as a function of $\sigma_{\tau_{1\,\mathrm{km}}}$ for cirrus 1 to 5. We see that $\Delta D_{\mathrm{eff\,1\,km}}$ are positive and increase, on average, with the cirrus mean optical thickness $\tau_\mathrm{c}$ (from cirrus 1 to 3) and the heterogeneity parameter $\rho_\tau$ (from cirrus 3 to 5). Indeed, in average, $\sigma_{\tau_{1\,\mathrm{km}}}$ increases with $\tau_\mathrm{c}$ and $\rho_\tau$, as expected.

Figure 8 is the same as Fig. 5 for different effective diameters: $D_\mathrm{eff}$ = 9.95 µm (cirrus 3), $D_\mathrm{eff}$ = 20.09 µm (cirrus 6) and $D_\mathrm{eff}$ = 40.58 µm (cirrus 7). The figure shows that $\Delta\varepsilon_\mathrm{eff}$ and $\Delta\tau_\mathrm{eff}$ decrease with the increase in $D_\mathrm{eff}$ (except at 8.65 µm where $\varpi_0$ increases between $D_\mathrm{eff}$ = 9.95 µm and 20.09 µm). Indeed, $\varpi_0$ increases with $D_\mathrm{eff}$ (except at 8.65 µm) and leads to a decrease of the absorption and, thus, of the PPA. The impact of the effective diameter on $\Delta\varepsilon_\mathrm{eff}$ and $\Delta\tau_\mathrm{eff}$ is particularly marked for the band at 12.05 µm where the absorption of ice crystals decreases strongly between $D_\mathrm{eff}$ = 9.95 µm (cirrus 3) and $D_\mathrm{eff}$ = 40.58 µm (cirrus 7).

In addition, we estimated the heterogeneity effects on the retrieved ice crystal effective diameters ($\Delta D_{\mathrm{eff\,1\,km}}$) for the three $D_\mathrm{eff}$. On average, $\Delta D_{\mathrm{eff\,1\,km}} \sim +3$ µm for cirrus 3 ($D_\mathrm{eff}$ = 9.95 µm) and 6 ($D_\mathrm{eff}$ = 20.09 µm). Thus, there is no a significant increase of heterogeneity effects on retrieved effective diameters between these two effective sizes. For cirrus 7 ($D_\mathrm{eff}$ = 40.58 µm), there is no real tendency ($\Delta D_{\mathrm{eff\,1\,km}} \sim \pm 0$ µm) due to the saturation of the SWT. Indeed, as notice above, effective diameters close to 40 µm lead to weak brightness temperature differences. This is illustrated in Fig. 2 where the amplitude of arches, and thus the sensitivity, decreases with the increase of the effective diameter.





AMTD
7, 8777–8816, 2014

## 3.2 Heterogeneity effects due to optical and microphysical property variabilities

As presented in Sect. 2.2, we use the parametrization developed by Baran et al. (2009); Baran (2012); Baran et al. (2013) to simulate a three-dimensional heterogeneous cloud optical property field from the 3-D distribution of the (IWC; temperature) couple. During the CIRCLE-2 campaign, values of IWC were measured and can be used, by combination with a mid-latitude summer temperature profile, to generate a realistic 3-D optical property field for the simulation of the cirrus (CII-1 and CII-2 cirrus). In addition, to compare with the previous cirrus, the cirrus CII-3 was generated from the cloudy field of the CIRCLE-2 cirrus but with the same optical properties than cirrus 8.

Figure 9 presents the impact of cirrus heterogeneities on the retrieved effective emissivity $\Delta\varepsilon_{\text{eff}}$ and on the effective optical thickness $\Delta\tau_{\text{eff}}$ as a function of the standard deviation of the optical thickness $\sigma_{\tau_{1\,\text{km}}}$ for cirrus CII-1, CII-2 and CII-3. $\Delta\varepsilon_{\text{eff}}$ and $\Delta\tau_{\text{eff}}$ are very close for the three cirrus, but we can see some slight differences as a function of the band. Indeed, at 8.65 µm, $\Delta\varepsilon_{\text{eff}}$ and $\Delta\tau_{\text{eff}}$ are smaller for the CII-3 cirrus than for the two others cirrus. At 10.60 µm, this difference is close to zero. At 12.05 µm, $\Delta\varepsilon_{\text{eff}}$ and $\Delta\tau_{\text{eff}}$ are larger for the CII-3 cirrus than for CII-1 and CII-2 cirrus. This effect is due to the variability of optical properties for cirrus CII-1 and cirrus CII-2. Indeed, cirrus CII-3 contains only aggregate crystals of effective diameter $D_{\text{eff}} = 9.95$ µm resulting from the model of Yang et al. (2001, 2005) while cirrus CII-1 and CII-2 contain crystal of various sizes. For CII-3 cirrus, small crystals have a single scattering albedo maximum at 8.65 µm, leading to a lower PPA bias. At 12.05 µm, as small particles are more absorbent in this band, the PPA is larger. Concerning the CII-1 cirrus, corresponding to the cirrus observed during the CIRCLE-2 campaign, the average error on the effective emissivity is in the limit of the method sensibility (Garnier et al., 2012) of about 0.03 in absolute value.

To study heterogeneity effects on the retrieved ice crystals effective diameters for CII-1 and CII-2 cirrus, we compare effective diameters $D_{\text{eff}}3\text{D}_{1\,\text{km}}$ and $\text{Deff}1\text{D}_{1\,\text{km}}$ retrieved from $BT3D_{1\,km}$ and $BT1D_{1\,km}$ respectively. $D_{eff}3D_{1\,km}$ and $\tau_{eff}3D_{1\,km}$ represents the cloud optical properties resulting of a 3-D radiative transfer through a heterogeneous atmosphere ($BT3D_{1\,km}$). The differences $\Delta D_{eff\,1\,km} = D_{eff}3D_{1\,km} - D_{eff}1D_{1\,km}$ and $\Delta\tau_{eff\ 1\,km} = \tau_{eff}3D_{1\,km} - \tau_{eff}1D_{1\,km}$ correspond, therefore, to the heterogeneity effects on the retrieval of $D_{eff}3D_{1\,km}$ and $\tau_{eff}$ 1 km. For these two cirrus, the optical properties are heterogeneneous. Therefore, we represent in Fig. 10a $\Delta D_{eff\,1\,km}$ as a function of $D_{eff}3D_{1\,km}$ and in Fig. 10b $\Delta\tau_{eff\ 1\,km}$ as a function of $\tau_{eff}3D_{1\,km}$. We see that $\Delta D_{eff\,1\,km}$ and $\Delta\tau_{eff\ 1\,km}$ increase, in absolute value, with $D_{eff}3D_{1\,km}$ and $\tau_{eff}3D_{1\,km}$ respectively. The Table 2, summarizes the optical properties retrieved by IIR during CIRCLE-2 and those retrieved from our simulations as well as the estimated heterogeneity effects. First of all, for cirrus CII-1, possessing the characteristics of the cirrus observed during the CIRCLE-2 campaign, the average value of the retrieved effective diameter $\overline{D_{eff}3D_{1\,km}} \sim 38.9\,\mu m$ and the mean effective optical thickness $\overline{\tau_{eff}3D_{1\,km}} \sim 0.40$ at 12.05 µm are close to those retrieved from the IIR measurements along the track of CALIOP / CALIPSO (without underlying liquid water cloud) of $D_{eff\,IIR} = 44.2\,\mu m$ and $\tau_{IIR} = 0.41$. There is, thus, a good agreement between optical properties retrieved by the IIR operational algorithm during the CIRCLE-2 campaign and those retrieved with our simulations. The mean error due to heterogeneity effects is approximately 5.1 µm (13 %) on the retrieved effective diameter and approximately −0.02, (5 %) on the effective optical thickness. In average, these relative errors due to heterogeneity effects are, thus, weak comparing to the incertitude estimate by Dubuisson et al. (2008) for the IIR retrieval (10 % to 25 % on $D_{eff\,1\,km}$ and 10 % on $\tau_{eff_{1\,km}}$). However, at the scale of the observation pixel, some values can reach more than 40 % on the effective diameter and 15 % on the effective optical thickness, which is quite significant. Furthermore, errors due to cloud heterogeneities increase with the IWC or the cirrus mean optical thickness, as for cirrus CII-2, having an IWC twice as big as cirrus CII-1, $\overline{\Delta D_{eff\,1\,km}} \sim 9.7\,\mu m$, (20 % in relative) and $\overline{\Delta\tau_{eff_{1\,km}}} \sim -0.05$ (7 % in relative).





AMTD
7, 8777–8816, 2014

Cirrus heterogeneities on thermal infrared optical properties

T. Fauchez et al.

### 3.3 Influence of the vertical variability of optical properties

To know the influence of the vertical variability of cirrus optical properties ($\sigma_e$, $\varpi_0$ and $g$) in the retrieval errors, we compare, for the CII-2 cirrus, cloud products retrieved from BT1D$_{1\,km}$ with vertically heterogeneous columns with those retrieved for vertically homogeneous columns obtained after a vertical averaging of the IWC.

Figures 11 show the effects of the vertical heterogeneity of the optical properties on the effective emissivity (a, b and c) and on the effective optical thickness (d, e and f) with $\varepsilon_{eff}1D_{he}$ and $\tau_{eff}1D_{he}$ the effective emissivity and the effective optical thickness, respectively, estimated from vertically heterogeneous cloudy columns and $\varepsilon_{eff}1D$ and $\tau_{eff}1D$ from vertically homogeneous cloudy columns as a function of the standard deviation of the optical thickness $\sigma_{\tau_{1\,km}}$, for the three IIR channels. Differences between retrieved products estimated from vertically heterogeneous and homogeneous cloudy columns are significantly weaker than those due to 3-D heterogeneities (horizontal and vertical heterogeneities). Furthermore, contrary to 3-D heterogeneity effects $\Delta\varepsilon_{eff}$ and $\Delta\tau_{eff}$, the differences ($\varepsilon_{eff}1D_{he} - \varepsilon_{eff}1D$) and ($\tau_{eff}1D_{he} - \tau_{eff}1D$) are positives. These effects are particular to our simulations, where vertical heterogeneities tend thus to smooth the heterogeneity effects. These observations can be explained with Fig. 12 representing the vertical profiles of the optical properties of cirrus CII-2 in the vertically heterogeneous case (red curves) an the vertically homogeneous case (black lines) after vertical averaging of the couple (IWC; Temperature) using the parametrization of Baran et al. (2009); Baran (2012); Baran et al. (2013). By this way, values of the vertically homogeneous case are different to the average of the optical coefficients of the vertically heterogeneous case: $\varpi_0$ of the vertically homogeneous case is larger than the vertical averaging of the heterogeneous case for bands at 10.60 µm and 12.05 µm. In addition, $g$ of the vertically homogeneous case is larger than the average of the vertically heterogeneous case in the three bands. Consequently, the cirrus is less absorbent in the vertically homogeneous case and thus the effective emissivities and effective optical thicknesses are weaker. This vertical variability of optical properties,



Discussion Paper | Discussion Paper | Discussion Paper | Discussion Paper |

AMTD

7, 8777–8816, 2014

Cirrus heterogeneities on thermal infrared optical properties

T. Fauchez et al.

for the cirrus CII-2, impact the retrieval of the effective diameter of, on average, 4 µm (figure not presented here).

## 4 Other sources of uncertainty

We show in the previous sections that heterogeneity effects can be an important source of errors on the retrieved optical properties. To compare its importance on the retrieved cloud parameters with regard to other sources of possible errors for IIR measurements, we test the impact of an incertitude of 1 K on the surface temperature and on the atmospheric temperature profile measurements. This error corresponds to that estimated by Garnier et al. (2012). Figure 13a shows the error on the retrieved effective diameter ΔDeff1D and Fig. 13b the error on the retrieved effective optical thickness $\Delta\tau_{\text{eff}}$1D according to $\tau_{\text{eff}}$1D for cirrus with a top altitude of 6 km, 8 km, 10 km and 12 km. The retrieval of the effective diameter and optical thickness is performed using the SWT for 1-D radiative transfer simulations. We can see that ΔDeff1D are less than 2.5 µm (25 %) and $\Delta\tau_{\text{eff}}$1D less than 0.16 (5 %). By comparison, these errors are in the IIR retrieval uncertainty of 10–25 % for $D_{\text{eff}}$ and about 10 % for $\tau_{\text{eff}}$ (Dubuisson et al., 2008). In addition, they are significantly weaker than those being able to be reached by cloud heterogeneity effects (more than 50 % for $D_{\text{eff}}$ and 10 % to 15 % for $\tau_{\text{eff}}$). In Fig. 13a, we see that the more the optical thickness of the cirrus and/or its top altitude increases, the less the error of 1 K on the temperature of surface affects the effective diameters. In Fig. 13b, the error on the atmospheric temperature profile increases with the optical thickness of the cirrus because its emissivity increases and therefore the impact of the temperature.

Fauchez et al. (2014) show that the cloud top altitude and geometrical thickness significantly influence the heterogeneity effects because the brightness temperature contrast between the surface and the cloud top increases with the cloud top altitude and decreases with the vertical extension for a constant cloud top (as the cloud base is closer





AMTD
7, 8777–8816, 2014
Cirrus heterogeneities on thermal infrared optical properties
T. Fauchez et al.

to the surface). For retrieved cloud products, the effective emissivity is independent of the cloud altitude and geometrical thickness, their impacts on the retrieval is weak.

## 5 Summary and conclusions

In this paper, we discussed on the impact of cirrus heterogeneity effects on the retrieval of cloud parameters from thermal infrared radiometric measurements from space. We have been focused on the IIR radiometer for which the operational algorithm estimates the cirrus effective emissivity, the effective optical thickness and the ice crystal effective diameter of the observation pixel. We show that errors due to the cirrus heterogeneity effects on the effective emissivity and the effective optical thickness are well correlated to the sub-pixel optical thickness standard deviation $\sigma_{\tau_{1\,\mathrm{km}}}$ and increase, in average, with the optical thickness $\tau_{1\,\mathrm{km}}$. These errors are greater than the precision of the retrieval method ($\Delta\varepsilon_{\mathrm{eff}} \sim 0.03$) for $\sigma_{\tau_{1\,\mathrm{km}}} \sim 1$, corresponding also to the value from which, heterogeneity effects on brightness temperatures become larger than the IIR instrumental accuracy of 1 K (Fauchez et al., 2014).

Our results are summarized in Table 3. Heterogeneity effects for three effective diameters are compared with the retrieval errors due to the vertical inhomogeneity of optical properties and with the impact of an error of 1 K, corresponding to the IIR accuracy, on the atmospheric temperature profile and on the surface temperature. Results are shown for pixels with $\sigma_{\tau_{1\,\mathrm{km}}} = 1$ (medium heterogeneity) and 2 (large heterogeneity). The most important errors on the cloud optical property retrieval concern those due to the sub-pixel heterogeneity of the optical thickness, in particular for the smallest crystals ($\overline{\Delta D_{\mathrm{eff}\,1\,\mathrm{km}}} = 2.5\,\mu\mathrm{m}$ ($\sim 25\,\%$) and $\Delta\tau_{\mathrm{eff}\ 1\,\mathrm{km}} = -0.20$ ($\sim 12\,\%$) for $\sigma_{\tau_{1\,\mathrm{km}}} = 1$). Indeed, the absorption is larger for small crystals and, thus, the PPA bias greater. For $D_{\mathrm{eff}} = 40.58\,\mu\mathrm{m}$, the crystal optical properties in the three channels converge to similar values leading to a slight brightness temperature differences between channels and, thus, to a decrease of the retrieval accuracy. Other possible sources of errors discussed in this paper are the vertical inhomogeneity of the optical properties, an error of 1 K on





AMTD
7, 8777–8816, 2014

the surface temperature or atmospheric temperature profile. They are all smaller than the IIR retrieval errors (Dubuisson et al., 2008). The influence of these parameters appears, thus, negligible regarding those relating to optical thickness heterogeneity and to the IIR retrieval incertitude.

The impact of cirrus heterogeneities on the retrieved cloud parameters studied in this paper are for a 1 km × 1 km spatial resolution. These biases could decrease with the increase of the spatial resolution of the spatial radiometer. However, photon transport effects increase with the spatial resolution. Fauchez et al. (2014) estimate that a spatial infrared radiometer with a resolution of 250 m × 250 m could significantly reduced the PPA bias while photon transport effects remain weak. Heterogeneity effects on the retrieved cloud products should be estimated for this configuration. This study gives also ways to potentially correct the heterogeneity errors using the subpixel measurements to estimate $\sigma_{\tau_{1\,\mathrm{km}}}$. Furthermore, differences between heterogeneity effects in the visible/near-infrared and thermal infrared ranges for different spatial resolutions could be investigated to estimate their impact on cloud products retrieved using a combination of the VNIR/SWIR and IR retrieval methods as that proposed by Cooper et al. (2007).

*Acknowledgements.* The authors acknowledge the Centre National de la Recherche Scientifique (CNRS), the Programme National de Télédétection Spatiale (PNTS) and the Direction Générale de l'Armement (DGA) for their financial support. We also thank the use of resources provided by the European Grid Infrastructure. For more information, please reference the EGI-InSPIRE paper (http://go.egi.eu/pdnon).

We thank Anthony Baran for the numerous fruitful discussions on the cirrus optical properties.

## References

Baran, A. J.: From the single-scattering properties of ice crystals to climate prediction: a way forward, Atmos. Res., 112, 45–69, 2012. 8782, 8790, 8792, 8801

Baran, A. J. and Labonnote, L.-C.: A self-consistent scattering model for cirrus. I: The solar region, Q. J. Roy. Meteor. Soc., 133, 1899–1912, 2007. 8782





AMTD

7, 8777–8816, 2014

Cirrus heterogeneities on thermal infrared optical properties

T. Fauchez et al.

Title Page

Abstract | Introduction

Conclusions | References

Tables | Figures

◂| |▸

◂ ▸

Back | Close

Full Screen / Esc

Printer-friendly Version

Interactive Discussion

Baran, A. J., Connolly, P. J., and Lee, C.: Testing an ensemble model of cirrus ice crystals using midlatitude in situ estimates of ice water content, volume extinction coefficient and the total solar optical depth, J. Quant. Spectrosc. Ra., 110, 1579–1598, 2009. 8782, 8790, 8792, 8801

Baran, A. J., Cotton, R., Furtado, K., Havemann, S., Labonnote, L.-C., Marenco, F., Smith, A., and Thelen, J.-C.: A self-consistent scattering model for cirrus. II: The high and low frequencies, Q. J. Roy. Meteor. Soc., 140, 1039–1057, doi:10.1002/qj.219, 2013. 8782, 8790, 8792, 8801

Baum, B., Yang, P., Heymsfield, A., Platnick, S., King, M., Hu, Y.-X., and Bedka, S.: Bulk scattering properties for the remote sensing of ice clouds. Part II. Narrowband models, J. Appl. Meteorol., 44, 1896–1911, 2005. 8782

Baum, B., Yang, P., Heymsfield, A., Schmitt, C., Xie, Y., Bansemer, A., Hu, Y.-X., and Zhang, Z.: Improvements in shortwave bulk scattering and absorption models for the remote sensing of ice clouds, J. Appl. Meteorol. Clim., 50, 1037–1056, 2011. 8782

C.-Labonnote, L., Brogniez, G., Doutriaux-Boucher, M., Buriez, J.-C., Gayet, J.-F., and Chepfer, H.: Modeling of light scattering in cirrus clouds with inhomogeneous hexagonal monocrystals. Comparison with in-situ and ADEOS-POLDER measurements, Geophys. Res. Lett., 27, 113–116, 2000. 8782

Cahalan, R. F., Ridgway, W., Wiscombe, W. J., Bell, T. L., and Snider, J. B.: The Albedo of Fractal Stratocumulus Clouds, J. Atmos. Sci., 51, 2434–2455, 1994. 8779

Carlin, B., Fu, Q., Lohmann, U., Mace, J., Sassen, K., and Comstock, J. M.: High cloud horizontal inhomogeneity and solar albedo bias, J. Climate, 15, 2321–2339, 2002. 8781

Cooper, S. J., L'Ecuyer, T. S., Gabriel, P., Baran, A. J., and Stephens, G. L.: Performance assessment of a five-channel estimation-based ice cloud retrieval scheme for use over the global oceans, J. Geophys. Res.-Atmos., 112, D042007, doi:10.1029/2006JD007122, 2007. 8780, 8795

Cornet, C., C.-Labonnote, L., and Szczap, F.: Three-dimensional polarized Monte Carlo atmospheric radiative transfer model (3DMCPOL): 3-D effects on polarized visible reflectances of a cirrus cloud, J. Quant. Spectrosc. Ra., 111, 174–186, doi:10.1016/j.jqsrt.2009.06.013, 2010. 8780, 8781, 8783

Dubuisson, P., Giraud, V., Chomette, O., Chepfer, H., and Pelon, J.: Fast radiative transfer modeling for infrared imaging radiometry, J. Quant. Spectrosc. Ra., 95, 201–220, 2005. 8785

Dubuisson, P., Giraud, V., Pelon, J., Cadet, B., and Yang, P.: Sensitivity of thermal infrared radiation at the top of the atmosphere and the surface to ice cloud microphysics., J. Appl. Meteorol. Clim., 47, 2545–2560, 2008. 8780, 8783, 8784, 8791, 8793, 8795, 8803

Fauchez, T., Cornet, C., Szczap, F, Dubuisson, P., and Rosambert, T.: Impact of cirrus clouds heterogeneities on top-of-atmosphere thermal infrared radiation, Atmos. Chem. Phys., 14, 5599–5615, doi:10.5194/acp-14-5599-2014, 2014. 8779, 8780, 8782, 8783, 8786, 8788, 8793, 8794, 8795

Field, P. R., Hogan, R. J., Brown, P. R. A., Illingworth, A. J., Choularton, T. W., and Cotton, R. J.: Parametrization of ice-particle size distributions for mid-latitude stratiform cloud, Q. J. Roy. Meteor. Soc., 131, 1997–2017, 2005. 8783

Field, P. R., Heymsfield, A., and Bansemer, A.: Snow size distribution parameterization for midlatitude and tropical ice clouds, J. Atmos. Sci., 64, 4346–4365, 2007. 8783

Garnier, A., Pelon, J., Dubuisson, P., Faivre, M., Chomette, O., Pascal, N., and Kratz, D. P.: Retrieval of cloud properties using CALIPSO imaging infrared radiometer. Part I: Effective emissivity and optical depth, J. Appl. Meteorol. Clim., 51, 1407–1425, 2012. 8779, 8783, 8784, 8788, 8790, 8793

Garnier, A., Pelon, J., Dubuisson, P., Yang, P., Faivre, M., Chomette, O., Pascal, N., Lucker, P., and Tim, M.: Retrieval of cloud properties using CALIPSO imaging infrared radiometer. Part II: Effective diameter and ice water path, J. Appl. Meteorol. Clim., 52, 2582–2599, 2013. 8779, 8781, 8782, 8783

Henyey, L. G. and Greenstein, J. L.: Diffuse radiation in the galaxy, Ann. Astrophys., 3, 117–137, 1940. 8782

Hogan, R. J. and Kew, S. F.: A 3-D stochastic cloud model for investigating the radiative properties of inhomogeneous cirrus clouds, Q. J. Roy. Meteor. Soc., 131, 2585–2608, 2005. 8781

Inoue, T.: On the temperature and effective emissivity determination of semi-transparent cirrus clouds by bi-spectral measurements in the 10 µm window region, J. Meteorol. Soc. Jpn., 63, 88–99, 1985. 8780, 8783

Katagiri, S., Sekiguchi, M., Hayasaka, T., and Nakajima, T.: Cirrus cloud radiative forcing at the top of atmosphere using the nighttime global distribution with the microphysical parameters derived from AVHRR, AIP Conf. Proc., 1531, 704–707, 2013. 8779

Kato, S. and Marshak, A.: Solar zenith and viewing geometry-dependent errors in satellite retrieved cloud optical thickness: marine stratocumulus case, J. Geophys. Res.-Atmos., 114, D01202, doi:10.1029/2008JD010579, 2009. 8780





AMTD

7, 8777–8816, 2014

Cirrus heterogeneities on thermal infrared optical properties

T. Fauchez et al.

Liou, K. N.: Influence of cirrus clouds on weather and climate processes: a global perspective, Mon. Weather Rev., 114, 1167–1199, 1986. 8779
Lynch, D. K., Sassen, K., Starr, D. O. C., and Stephens, G.: Cirrus, Oxford University Press, USA, 2002. 8781
Magono, C.: Meteorological Classification of Natural Snow Crystals, Hokkaido University, 1966. 8782
Marshak, A. and Davis, A. A. B.: 3-D Radiative Transfer in Cloudy Atmospheres, Physics of Earth and Space Environments Series, Springer-Verlag, Berlin Heidelberg, 2005. 8783
Mayer, B.: Radiative transfer in the cloudy atmosphere, Eur. Phys. J. Conferences, 1, 75–99, 2009. 8783
Mioche, G., Josset, D., Gaye, J. F., Pelon, J., Garnier, A., Minikin, A., and Schwarzenboeck, A.: Validation of the CALIPSO-CALIOP extinction coefficients from in situ observations in midlatitude cirrus clouds during the CIRCLE-2 experiment, J. Geophys. Res.-Atmos., 115, D00H25, doi:10.1029/2009JD012376, 2010. 8782
Nakajima, T. and King, M. D.: Determination of the optical thickness and effective particle radius of clouds from reflected solar radiation measurements. Part I: Theory, J. Atmos. Sci., 47, 1878–1893, 1990. 8780
Parol, F., Buriez, J. C., Brogniez, G., and Fouquart, Y.: Information content of AVHRR channels 4 and 5 with respect to the effective radius of cirrus cloud particles, J. Appl. Meteorol., 30, 973–984, 1991. 8780, 8783
Platnick, S., King, M. D., Ackerman, S. A., Menzel, W. P., Baum, B. A., Riedi, J. C., and Frey, R. A.: The MODIS cloud products: algorithms and examples from terra, IEEE T. Geosci. Remote, 41, 459–473, 2003. 8779
Radel, G., Stubenrauch, C. J., Holz, R., and Mitchell, D. L.: Retrieval of effective ice crystal size in the infrared: sensitivity study and global measurements from TIROS-N Operational Vertical Sounder, J. Geophys. Res.-Atmos., 108, 4281, doi:10.1029/2002JD002801, 2003. 8783
Rienecker, M. M., Suarez, M. J., Todling, R., Bacmeister, J., Takacs, L., Liu, H.-C., Gu, W., Sienkiewicz, M., Koster, R. D., Gelaro, R., Stajner, I., and Nielsen, J. E.: Technical Report Series on Global Modeling and Data Assimilation, Technical Report, 27, 2008. 8784
Sassen, K. and Cho, B. S.: Subvisual-thin cirrus lidar dataset for satellite verification and climatological research, J. Appl. Meteorol., 31, 1275–1285, 1992. 8781

Sourdeval, O., Brogniez, G., Pelon, J., C.-Labonnote, L., Dubuisson, P., Parol, F., Josset, D., Garnier, A., Faivre, M., and Minikin, A.: Validation of IIR/CALIPSO level 1 measurements by comparison with collocated airborne observations during CIRCLE-2 and Biscay '08 campaigns, J. Atmos. Ocean. Tech., 29, 653–667, 2012. 8784

Starr, D. O. and Cox, S. K.: Cirrus clouds. Part II: Numerical experiments on the formation and maintenance of cirrus, J. Atmos. Sci., 42, 2682–2694, 1985. 8781

Stephens, G. L.: Radiative properties of cirrus clouds in the infrared region, J. Atmos. Sci., 37, 435–446, 1980. 8779

Stephens, G. L., Gabriel, P. M., and Tsay, S.-C.: Statistical radiative transport in one-dimensional media and its application to the terrestrial atmosphere, Transport Theor. Stat., 20, 139–175, 1991. 8779

Szczap, F., Isaka, H., Saute, M., Guillemet, B., and Gour, Y.: Inhomogeneity effects of 1-D and 2-D bounded cascade model clouds on their effective radiative properties, Phys. Chem. Earth Pt. B, 25, 83–89, 2000. 8781

Szczap, F., Gour, Y., Fauchez, T., Cornet, C., Faure, T., Jourdan, O., and Dubuisson, P.: A flexible three-dimensional stratocumulus, cumulus and cirrus cloud generator (3DCLOUD) based on drastically simplified atmospheric equations and Fourier transform framework, Geosci. Model Dev. Discuss., 7, 295–337, doi:10.5194/gmdd-7-295-2014, 2014. 8780, 8781

Varnai, T. and Marshak, A.: Statistical analysis of the uncertainties in cloud optical depth retrievals caused by three-dimensional radiative effects, J. Atmos. Sci., 58, 1540–1548, 2001. 8780

Vaughan, M. A., Powell, K. A., Kuehn, R. E., Young, S. A., Winker, D. M., Hostetler, C. A., Hunt, W. H., Liu, Z., McGill, M. J., and Getzewich, B. J.: Fully automated detection of cloud and aerosol layers in the CALIPSO lidar measurements, J. Atmos. Ocean. Tech., 26, 2034–2050, 2009. 8785

Yang, P., Gao, B.-C., Baum, B. A., Hu, Y. X., Wiscombe, W. J., Tsay, S.-C., Winker, D. M., and Nasiri, S. L.: Radiative properties of cirrus clouds in the infrared (8–13 µm) spectral region, J. Quant. Spectrosc. Ra., 70, 473–504, 2001. 8782, 8785, 8790, 8801

Yang, P., Wei, H., Huang, H.-L., Baum, B. A., Hu, Y. X., Kattawar, G. W., Mishchenko, M. I., and Fu, Q.: Scattering and absorption property database for nonspherical ice particles in the near- through far-infrared spectral region, Appl. Optics, 44, 5512–5523, 2005. 8782, 8785, 8790, 8801

Zinner, T. and Mayer, B.: Remote sensing of stratocumulus clouds: uncertainties and biases due to inhomogeneity, J. Geophys. Res.-Atmos., 111, D14209, doi:10.1029/2005JD006955, 2006. 8780

**Table 1.** Mean cloud properties of the cirrus generated by 3DCLOUD. "CTA" corresponds to the Cirrus Top Altitude, "OP" corresponds to the optical properties parametrization, with "Yal" representing the model of ice crystals developed by Yang et al. (2001, 2005) for aggregates ice crystals and "Bal" represents the parametrization of ice crystals optical properties developed by Baran et al. (2009, 2013) and Baran (2012), $\tau_c$ is the cloud mean optical thickness, $\sigma_\tau$ the cloud standard deviation of the optical thickness estimated from the optical thickness of the subpixels at the scale of 100 m × 100 m, $\rho_\tau$ the cloud heterogeneity parameter define as the ratio of $\sigma_\tau$ by $\tau_c$ and $D_{\text{eff}}$ the ice crystal effective diameter.

| Cirrus | CTA (km) | $\tau_c$ | $\sigma_\tau$ | $\rho_\tau$ | $D_{\text{eff}}$ (µm) | OP |
|---|---|---|---|---|---|---|
| 1 | 7.97 | 0.45 | 0.32 | 0.7 | 9.95 | Yal |
| 2 | 7.97 | 0.90 | 0.63 | 0.7 | 9.95 | Yal |
| 3 | 7.97 | 1.80 | 1.26 | 0.7 | 9.95 | Yal |
| 4 | 7.97 | 1.80 | 1.98 | 1.1 | 9.95 | Yal |
| 5 | 7.97 | 1.80 | 2.70 | 1.5 | 9.95 | Yal |
| 6 | 7.97 | 1.80 | 1.26 | 0.7 | 20.09 | Yal |
| 7 | 7.97 | 1.80 | 1.26 | 0.7 | 40.58 | Yal |
| 8 | 11.06 | 0.90 | 0.63 | 0.7 | 9.95 | Yal |
| CIRCLE II 1 | 11.06 | 0.41 | 0.32 | 0.77 | Heterogeneous | Bal |
| CIRCLE II 2 | 11.06 | 0.81 | 0.62 | 0.77 | Heterogeneous | Bal |
| CIRCLE II 3 | 11.06 | 0.90 | 0.63 | 0.70 | 9.95 | Yal |





AMTD
7, 8777–8816, 2014

**Table 2.** $\overline{D_{\mathrm{eff_{IIR}}}}$ and $\overline{\tau_{\mathrm{IIR}}}$: averaged effective diameter and optical thickness, respectively, retrieved by IIR, on the 25 May 2007 during the CIRCLE-2 campaign; $\overline{D_{\mathrm{eff}}3\mathrm{D}_{1\,\mathrm{km}}}$ and $\overline{\tau 3\mathrm{D}_{1\,\mathrm{km}}}$: averaged effective diameter and optical thickness, respectively, retrieved for CII-1 and CII-2 cirrus and $\overline{\Delta D_{\mathrm{eff}}3\mathrm{D}_{1\,\mathrm{km}}}$ and $\overline{\Delta\tau 3\mathrm{D}_{1\,\mathrm{km}}}$: averaged errors on the effective diameter and optical thickness, respectively, due to cloud heterogeneities in absolute value and in percentage.

| Cirrus | $\overline{D_{\mathrm{eff_{IIR}}}}$ (µm) | $\overline{D_{\mathrm{eff}}3\mathrm{D}_{1\,\mathrm{km}}}$ (µm) | $\overline{\Delta D_{\mathrm{eff}}3\mathrm{D}_{1\,\mathrm{km}}}$ (µm) | $\overline{\tau_{\mathrm{IIR}}}$ | $\overline{\tau 3\mathrm{D}_{1\,\mathrm{km}}}$ | $\overline{\Delta\tau 3\mathrm{D}_{1\,\mathrm{km}}}$ |
|---|---|---|---|---|---|---|
| CII-1 | 44.2 | 38.9 | 5.1 (13 %) | 0.41 | 0.40 | −0.02 (−5 %) |
| CII-2 | – | 48.7 | 9.7 (20 %) | – | 0.74 | −0.05 (−7 %) |





AMTD
7, 8777–8816, 2014

**Table 3.** Averaged errors on the retrieved cirrus optical properties due to: the 3-D cloud heterogeneity for three ice crystal effective diameters (columns 3, 4 and 5); due to the vertical heterogeneity of optical properties (Vert. hetero., column 6) with $1D_{vhe}$ and $1D_{vho}$ representing the 1-D radiative transfer with vertically heterogeneous and homogeneous columns respectively; due to an incertitude of 1 K on the surface temperature (column 7) and on the temperature atmospheric profile (column 8) and due to the incertitude of the IIR retrieval (Dubuisson et al., 2008, column 9). $\overline{\Delta D_{\mathrm{eff}_{1\,\mathrm{km}}}}$ and $\overline{|\Delta D_{\mathrm{eff}_{1\,\mathrm{km}}}|}$ correspond to the absolute error in micrometers and to the relative error in percent, respectively, on the retrieval of the effective diameter; $\overline{\Delta \tau_{1\,\mathrm{km}}}$ and $\overline{|\Delta \tau_{1\,\mathrm{km}}|}$ correspond to the absolute and relative error in percent, respectively, on the retrieval of the optical thickness.

| | | Horizontal heterogeneity effects as a function of $D_{\mathrm{eff}}$ | | | Vert. hetero. (1Dvhe – 1Dvho) | Others uncertainties Surface 1 K | Atmosphere 1 K | IIR uncertainty |
|---|---|---|---|---|---|---|---|---|
| $\sigma_{\tau_{1\,\mathrm{km}}}$ | $D_{\mathrm{eff}}$ (µm) | 40.58 | 20.09 | 9.95 | 48.7 | 9.95 | 9.95 | – |
| 1 | $\overline{\Delta D_{\mathrm{eff}_{1\,\mathrm{km}}}}$ (µm) | −0.5 | 2.0 | 2.5 | 2 | 1 | 0.2 | – |
| | $\overline{\lvert\Delta D_{\mathrm{eff}_{1\,\mathrm{km}}}\rvert}$ (%) | ∼ 1 | ∼ 10 | ∼ 25 | ∼ 4 | ∼ 10 | ∼ 2 | ∼ 10 to ∼ 25 |
| | $\overline{\Delta \tau_{\mathrm{eff}\ 1\,\mathrm{km}}}$ | −0.02 | −0.10 | −0.20 | 0.03 | 0.04 | 0.08 | – |
| | $\overline{\lvert\Delta \tau_{\mathrm{eff}\ 1\,\mathrm{km}}\rvert}$ (%) | ∼ 1 | ∼ 6 | ∼ 12 | ∼ 4 | ∼ 2 | ∼ 4 | ∼ 10 |
| 2 | $\overline{\Delta D_{\mathrm{eff}_{1\,\mathrm{km}}}}$ (µm) | 1 | 3 | 3 | 2 | – | – | – |
| | $\overline{\lvert\Delta D_{\mathrm{eff}_{1\,\mathrm{km}}}\rvert}$ (%) | ∼ 3 | ∼ 15 | ∼ 40 | ∼ 4 | – | – | ∼ 10 to ∼ 25 |
| | $\overline{\Delta \tau_{\mathrm{eff}\ 1\,\mathrm{km}}}$ | −0.10 | −0.20 | −0.50 | 0.10 | – | – | – |
| | $\overline{\lvert\Delta \tau_{\mathrm{eff}\ 1\,\mathrm{km}}\rvert}$ (%) | ∼ 6 | ∼ 12 | ∼ 28 | ∼ 12 | – | – | ∼ 10 |





AMTD
7, 8777–8816, 2014

Cirrus heterogeneities on thermal infrared optical properties

T. Fauchez et al.

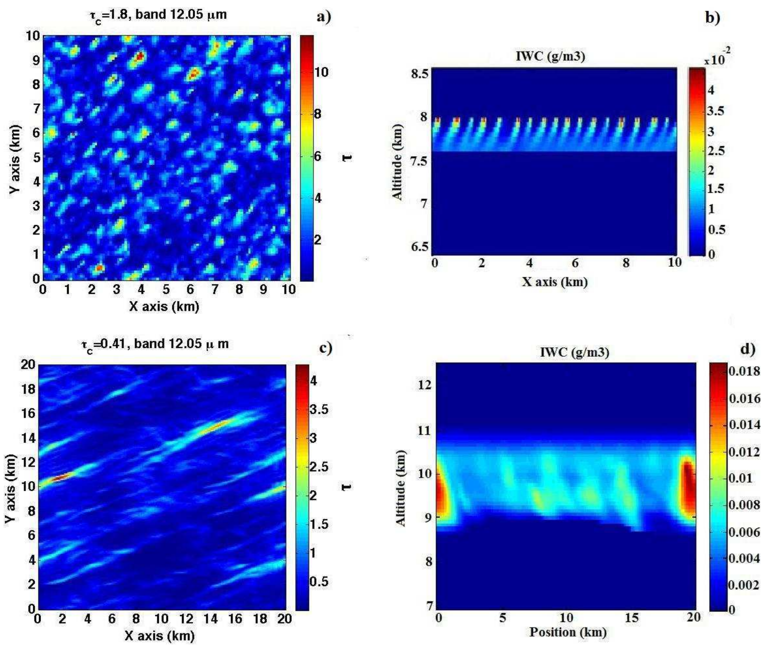


**Figure 1.** Top figures: cirrus generated from realistic meteorological conditions (Starr and Cox, 1986; Hogan and Kew, 2005) with **(a)** the 10 km × 10 km optical thickness field simulated at 12.05 µm with a horizontal spatial resolution of 100 m and **(b)** the *x*–*z* view of the cirrus IWC with a vertical spatial resolution of 58 m. Bottom figures: CII cirrus generated from measurements of the cirrus observed during the CIRCLE-2 campaign the 25 may 2007: **(c)** the 20 km × 20 km optical thickness field at 12.05 µm with a horizontal spatial resolution of 100 m and with a mean optical thickness $\tau_c = 0.41$ observed by IIR at 12.05 µm and **(d)** represents the *x*–*z* view of the cirrus IWC with a vertical resolution of 58 m.





AMTD
7, 8777–8816, 2014

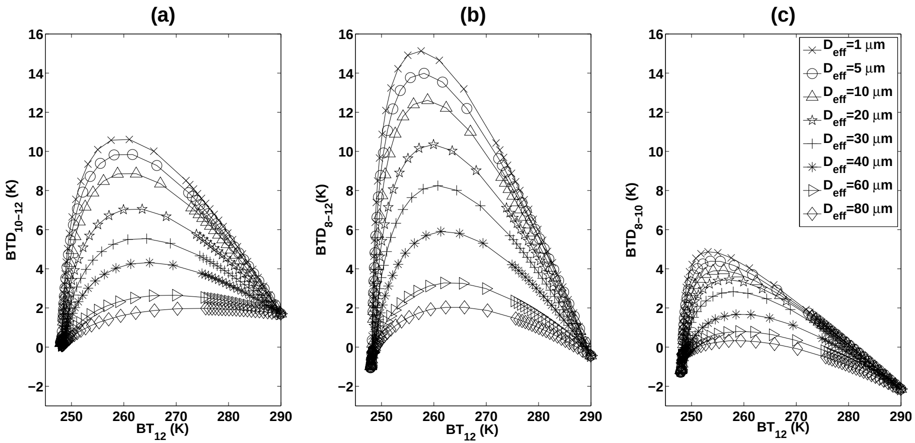


**Figure 2.** Brightness Temperatures Differences (BTD) as a function of the 12.05 µm BT ($BT_{12}$) for eight effective diameters $D_{\text{eff}}$ and different optical thickness between 0 to 50 at 12.05 µm. **(a)** $BTD_{10-12}$ between 10.60 µm – 12.05 µm channels, **(b)** $BTD_{8-12}$ between 8.65 µm – 12.05 µm channels, **(c)** $BTD_{8-10}$ between 8.65 µm – 10.60 µm channels.





AMTD
7, 8777–8816, 2014

Cirrus heterogeneities on thermal infrared optical properties

T. Fauchez et al.

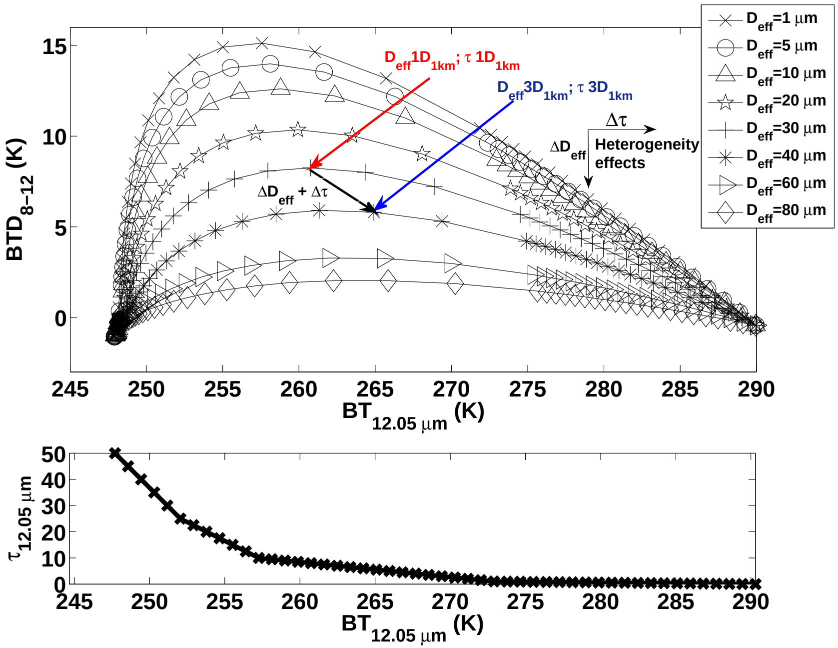


**Figure 3.** Top panel: Brightness Temperature Differences between 8.65 µm and 12.05 µm ($BTD_{12–8}$) as a function of the Brightness Temperature at 12.05 µm ($BT_{12}$). The red arrow shows an example of effective diameter $D_{\text{eff}}1D_{1\,\text{km}}$ and optical thickness $\tau 1D_{1\,\text{km}}$ retrieved in 1-D without heterogeneity effects and the blue arrow shows the corresponding effective diameter $D_{\text{eff}}3D_{1\,\text{km}}$ and optical thickness $\tau 3D_{1\,\text{km}}$ retrieved with heterogeneity effects. Heterogeneity effects $\Delta D_{\text{eff}}$ and $\Delta\tau$ lead to an overestimation of the effective diameter and to an underestimaton of the optical thickness respectively. At each point of the arches correspond an optical thickness represented in the bottom pannel, with $\tau_{12.05\,\mu\text{m}}$ the optical thickness at 12.05 µm.





AMTD
7, 8777–8816, 2014

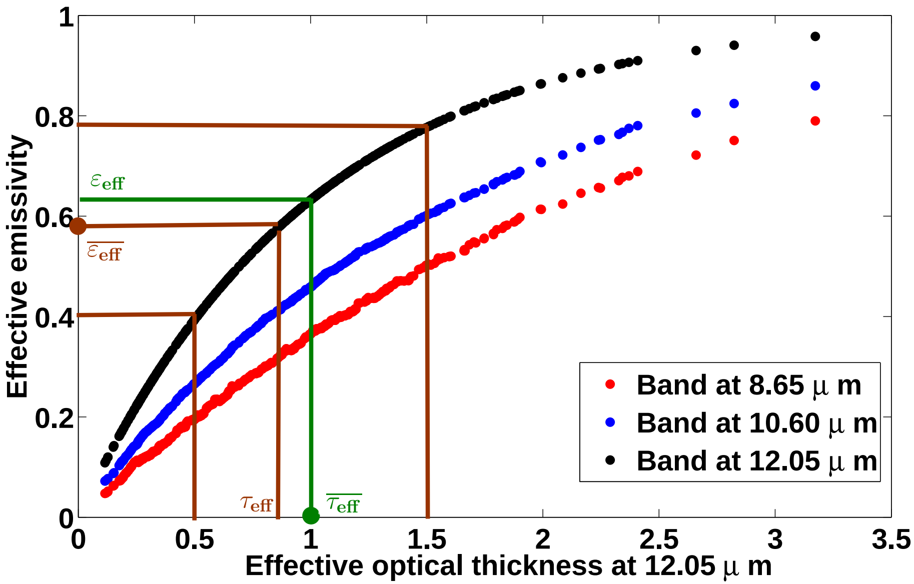


**Figure 4.** Variation of the effective emissivity as a function of the effective optical thickness at 12.05 µm estimated in 1-D at the spatial resolution of 100 m for the three IIR channels and for cloudy pixels belonging to cirrus 1 to 5. $\tau_{\rm eff}$ represents the effective optical thickness corresponding to the averaged effective emissivity $\overline{\varepsilon_{\rm eff}}$, $\overline{\tau_{\rm eff}}$ represents the averaged effective optical thickness and $\varepsilon_{\rm eff}$ its correspondent effective emissivity. The mathematical formulation of the PPA due to the Jensen inequality is expressed by: $\overline{\varepsilon_{\rm eff}} < \varepsilon_{\rm eff}(\overline{\tau_{\rm eff}})$.





AMTD
7, 8777–8816, 2014

Cirrus heterogeneities on thermal infrared optical properties

T. Fauchez et al.

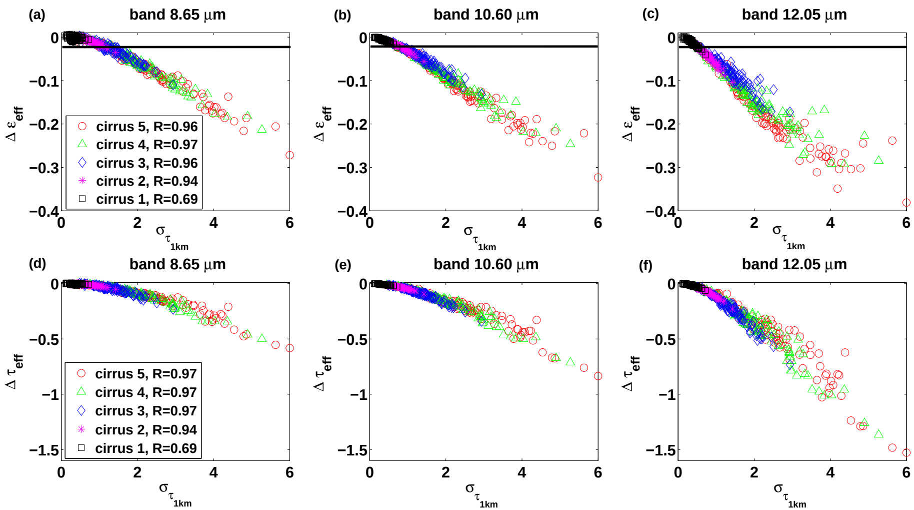


**Figure 5.** Error on the effective emissivity $\Delta\varepsilon_{\text{eff}}$ **(a–c)** and on the effective optical thickness $\Delta\tau_{\text{eff}}$ **(d–f)** at 8.65 µm, 10.60 µm and 12.05 µm respectively, as a function of the optical thickness standard deviation $\sigma_{\tau_{1\,\text{km}}}$ for cirrus 1 ($\tau_c = 0.45$, $\rho_\tau = 0.7$), 2 ($\tau_c = 0.90$, $\rho_\tau = 0.7$), 3 ($\tau_c = 1.80$, $\rho_\tau = 0.7$), 4 ($\tau_c = 1.80$, $\rho_\tau = 1.1$) and 5 ($\tau_c = 1.80$, $\rho_\tau = 1.5$) with $D_{\text{eff}} = 9.95$ µm for the five cirrus. The black lines correspond to the IIR operational algorithm uncertainty on the effective emissivity.





AMTD
7, 8777–8816, 2014

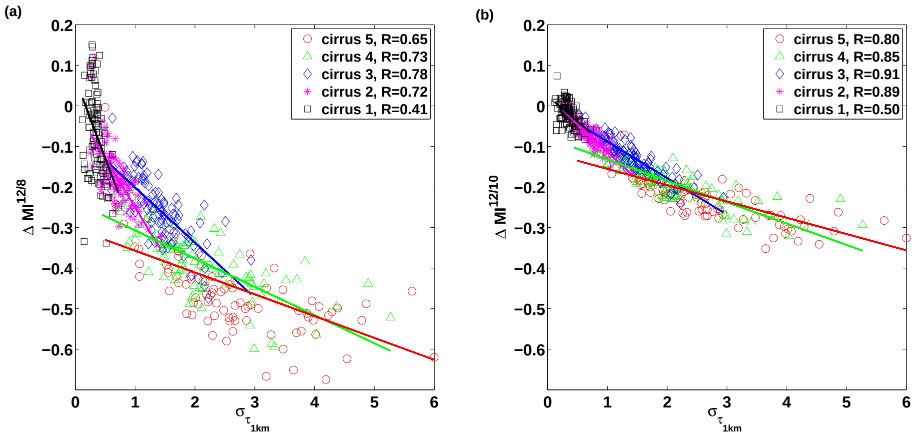


**Figure 6.** Microphysical index differences $\Delta MI^{12/8}$ **(a)** and $\Delta MI^{12/10}$ **(b)** as a function of the standard deviation of the optical thickness $\sigma_{\tau_{1\,km}}$ for cirrus 1 ($\tau_c = 0.45$, $\rho_\tau = 0.7$), 2 ($\tau_c = 0.90$, $\rho_\tau = 0.7$), 3 ($\tau_c = 1.80$, $\rho_\tau = 0.7$), 4 ($\tau_c = 1.80$, $\rho_\tau = 1.1$) and 5 ($\tau_c = 1.80$, $\rho_\tau = 1.5$) with $D_{eff}$ = 9.95 µm for the five cirrus.





AMTD
7, 8777–8816, 2014

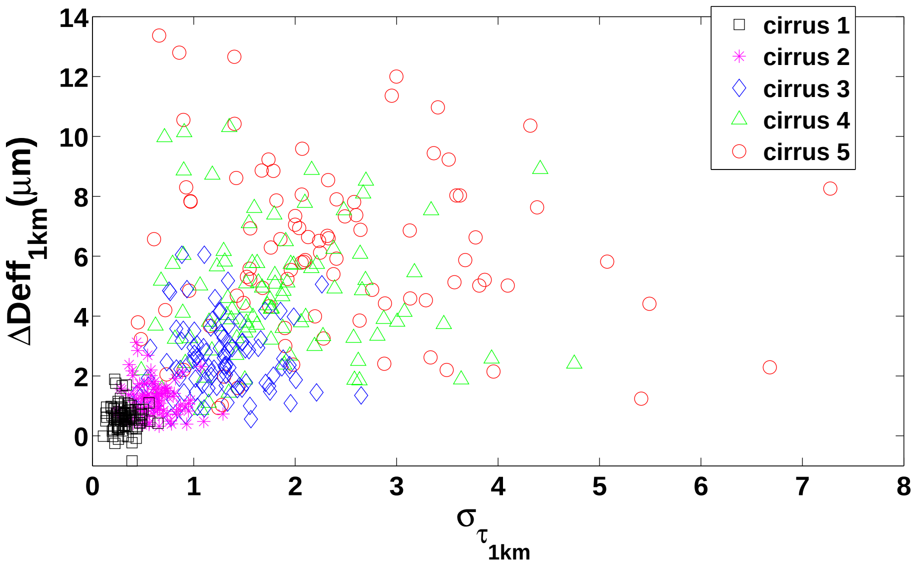


**Figure 7.** Error on the retrieved effective diameter $\Delta D_{\mathrm{eff\,1\,km}}$ as a function of the standard deviation of the optical thickness $\sigma_{\tau_{1\,\mathrm{km}}}$ for cirrus 1 ($\tau_c = 0.45$, $\rho_\tau = 0.7$), 2 ($\tau_c = 0.90$, $\rho_\tau = 0.7$), 3 ($\tau_c = 1.80$, $\rho_\tau = 0.7$), 4 ($\tau_c = 1.80$, $\rho_\tau = 1.1$) and 5 ($\tau_c = 1.80$, $\rho_\tau = 1.5$) with $D_{\mathrm{eff}} = 9.95$ µm for the five cirrus. Effective diameters are estimated using the Split Window Technique.





AMTD
7, 8777–8816, 2014

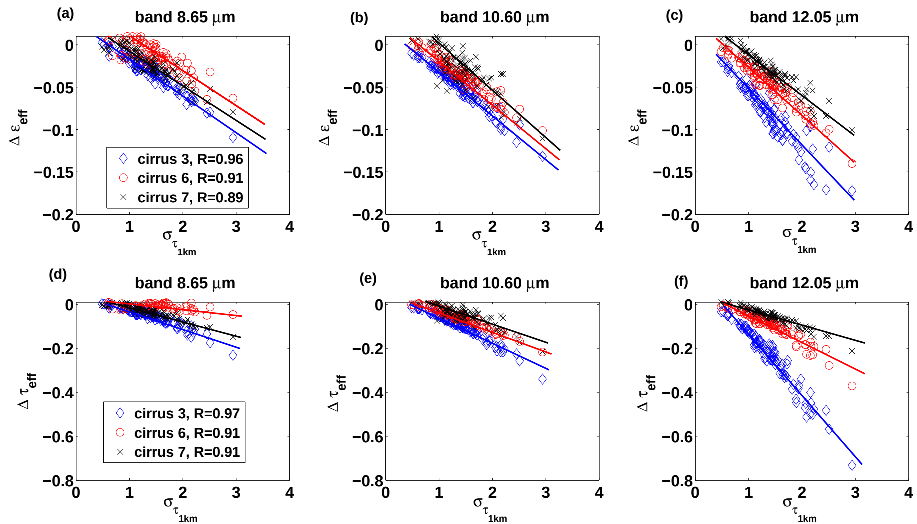


**Figure 8.** Error on the effective emissivity $\Delta\varepsilon_{\mathrm{eff}}$ **(a–c)** and on the effective optical thickness $\Delta\tau_{\mathrm{eff}}$ **(d–f)** at 8.65 µm, 10.60 µm and 12.05 µm respectively, as a function of the optical thickness standard deviation $\sigma_{\tau_{1\,\mathrm{km}}}$ for three indentical cirrus fields but for different ice crystal effective diameters: cirrus 3 ($D_{\mathrm{eff}}$ = 9.95 µm), cirrus 6 ($D_{\mathrm{eff}}$ = 20.09 µm) et cirrus 7 ($D_{\mathrm{eff}}$ = 40.58 µm) with $\tau_{\mathrm{c}}$ = 1.80 and $\rho_{\tau}$ = 0.7 for the three cirrus.





AMTD
7, 8777–8816, 2014

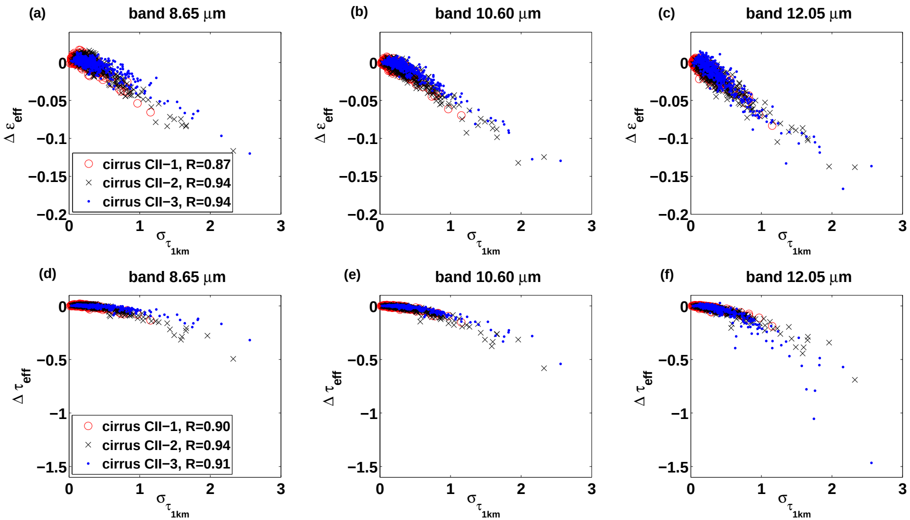


**Figure 9.** Error on the effective emissivity $\Delta\varepsilon_{\text{eff}}$ **(a–c)** and on the effective optical thickness $\Delta\tau_{\text{eff}}$ **(d–f)** at 8.65 µm, 10.60 µm and 12.05 µm respectively, as a function of the optical thickness standard deviation $\sigma_{\tau_{1\,\text{km}}}$ for cirrus CII-1, CII-2 and CII-3.





AMTD
7, 8777–8816, 2014

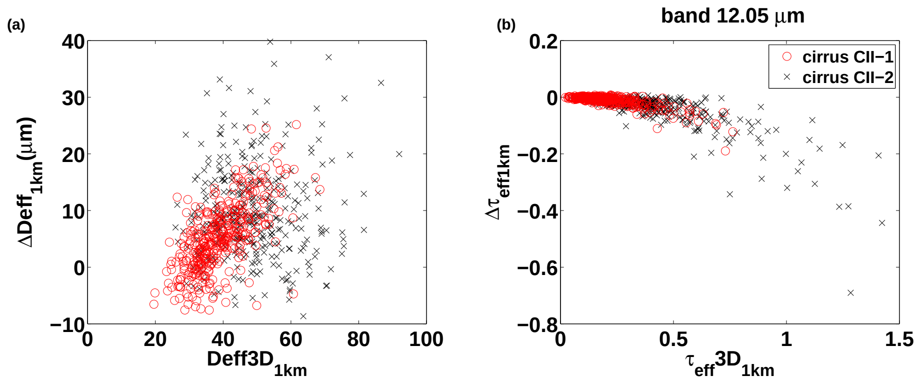


**Figure 10. (a)** Error on the retrieved effective diameter $\Delta D_{\mathrm{eff\,1\,km}}$ as a function of the effective diameter $D_{\mathrm{eff}}3\mathrm{D}_{1\,\mathrm{km}}$ and **(b)** error on the effective optical thickness $\Delta\tau_{\mathrm{eff\ 1\,km}}$ as a function of the effective optical thickness $\tau_{\mathrm{eff}}3\mathrm{D}_{1\,\mathrm{km}}$ for cirrus CII-1 et CII-2.





AMTD
7, 8777–8816, 2014

Cirrus heterogeneities on thermal infrared optical properties

T. Fauchez et al.

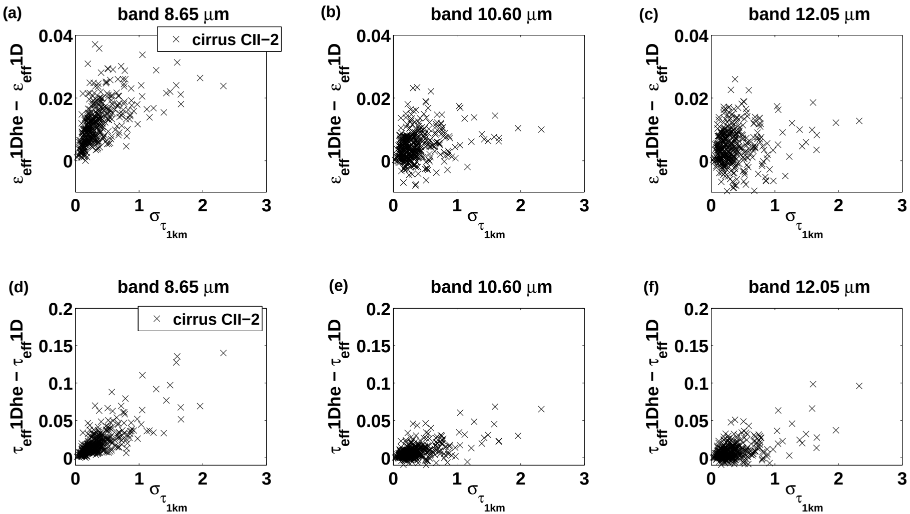


**Figure 11.** Effective emissivity differences **(a–c)** between $\varepsilon_{\text{eff}}1\text{D}_{\text{he}}$ and $\varepsilon_{\text{eff}}1\text{D}$ and effective optical thickness differences **(d–f)** between $\tau_{\text{eff}}1\text{D}_{\text{he}}$ and $\tau_{\text{eff}}1\text{D}$ retrieved from radiances calculated in the case of vertically heterogeneous and vertically homogeneous cloudy columns respectively as a function of the standard deviation of the optical thickness $\sigma_{\tau_{1\,\text{km}}}$ for cirrus CII-2 for bands at 8.65 µm, 10.60 µm and 12.05 µm respectively.





AMTD
7, 8777–8816, 2014

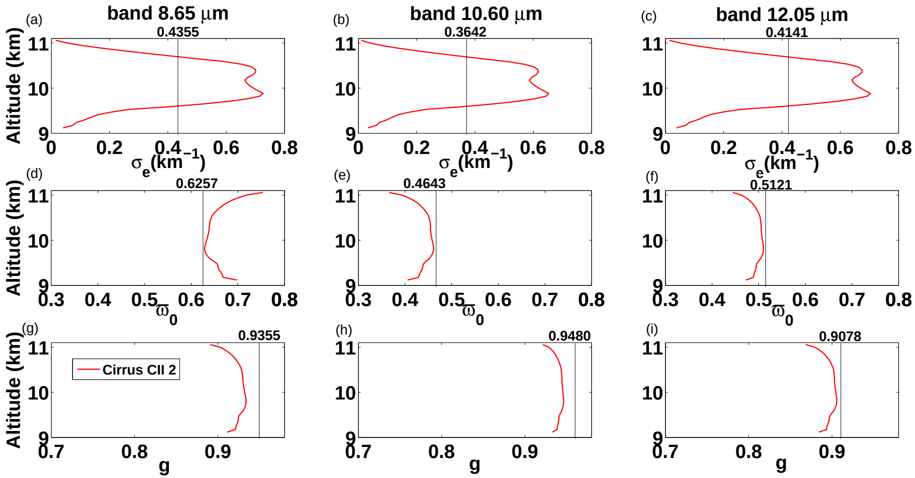


**Figure 12. (a–c)**: Vertical variation of the mean extinction coefficient $\sigma_e$; **(d–f)**: vertical variation of the mean single scattering albedo $\varpi_0$; **(g–i)**: vertical variation of the assymetry factor $g$ for the three IIR channels at 8.65 µm, 10.60 µm and 12.05 µm for cirrus CII-2. Vertical black lines correspond to the mean value of the optical coefficient obtained after vertical averaging of the IWC.





AMTD
7, 8777–8816, 2014

Cirrus heterogeneities on thermal infrared optical properties

T. Fauchez et al.

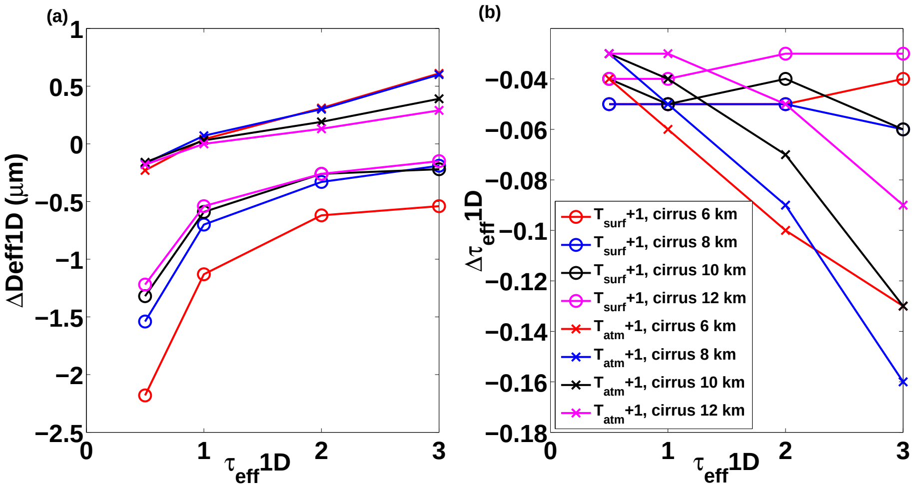


**Figure 13.** Errors on the **(a)** retrieved effective diameter $\Delta D_{\text{eff}}$1D and **(b)** on the effctive optical thickness $\Delta\tau_{\text{eff}}$1D as a function of $\tau_{\text{eff}}$1D due to an error of +1 K on the surface temperature ($T_{\text{surf}}+1$) and +1 K on the atmospheric temperature profile ($T_{\text{atm}}+1$) for cirrus with top altitudes of 6 km, 8 km, 10 km and 12 km.